JOURNAL OF MATERIALS SCIENCE 27 (1992) 3939–3952

Nanoindentation experiments on some amorphous hydrogenated carbon (a-C:H) thin films on silicon

J. C. KNIGHT, A. J. WHITEHEAD, T. F. PAGE
Materials Division, Department of Mechanical, Materials and Manufacturing Engineering, The University, Newcastle upon Tyne NE1 7RU, UK

Ultra-low-load indentation (nanoindentation) experiments have been used to investigate the load–displacement characteristics of two types of hydrogenated carbon films (a "hard" and a "soft" version ~230 and ~210 nm thick, respectively) deposited from methane on to (1 0 0) single-crystal silicon wafers by a radio frequency plasma-assisted chemical vapour deposition process. Further, the technique was used to explore the changes in the properties of the films with heat treatment in vacuum at temperatures of up to 650 °C. In all cases, the elastic and plastic properties of the films were compared at indentation loads in the range 0–60 mN, the higher loads causing indentor displacements greater than the thickness of the films. For the harder, stiffer coating, penetration resistance was found to decrease with increasing indenter displacement, reflecting the greater load-carrying role taken by the softer silicon with increasing applied load. However, for the softer coating, penetration resistance generally increased with displacement, perhaps reflecting progressive compaction of the coating in addition to the increasing role of the silicon. In both cases, heat treatment severely degraded the mechanical properties of the films due to thermally induced chemical changes and, in the case of the "hard" coating, relaxation of residual stresses. Scanning electron microscopy of both nanoindentations and low-load microhardness indentations clearly reveals the deformation mechanisms associated with contact stresses to include flow and fracture of the film and interfacial decohesion.

1. Introduction

In the past, conventional microhardness testing has been widely used to explore the near-surface mechanical properties of surface engineered solids such as thin-film coated systems and ion-implanted materials [1–4]. Recently, however, ultra-low-load indentation testing (nanoindentation) techniques have been used increasingly to overcome the limitations of microhardness testing both in examining the properties of very thin films and exploring surface deformation mechanisms at the fine scales relevant to wear. For example, the depth of even the smallest Vickers and Knoop microindentations reliably measurable by light microscopy is often greater than, or of the order of, the thickness of the coating or implanted layer and thus gives hardness values which are often some composite value of the coating and the substrate [2, 3]. Further, because *post facto* measurements of the size of the remnant impression are involved, it is usually difficult to separate fully the elastic and plastic components of the indentation response or examine any variation in properties through the coating thickness.

Current nanoindentation methods are capable of probing surface and near-surface mechanical properties of materials [5–9]. In such experiments the load and displacement of the indenter are continuously and simultaneously recorded to very high levels of accuracy (e.g. 0.3 μN and 0.16 nm). Such nanoindentation techniques are powerful and elegant in that not only can the mechanical properties (e.g. elastic and plastic characteristics, hardness, penetration resistance) of the coating or modified surface layer be determined *in situ* (i.e. in the microstructural and residual stress state in which the substrate–coating composite is used), but also any changes in properties through the coating thickness can sometimes be investigated. Further, at small penetration depths compared to the thickness of the coating, it is possible to investigate the properties of the coating in virtual isolation from the substrate. Thus, data generated by the technique can be used to assess the contact response and wear performance of coated systems as well as a means of monitoring coating quality (for example, in terms of point to point reliability).

In this work, nanoindentation has been employed to determine the nanoscale mechanical properties of two different amorphous hydrogenated carbon (a-C:H) films (a "hard" and a "soft" version) deposited on single-crystal (1 0 0) silicon wafers by a radio frequency plasma-assisted chemical vapour deposition (r.f.-PACVD) method. Changes in properties induced by annealing in vacuum at temperatures up to 650 °C have been explored. Furthermore, high-resolution scanning electron microscopy and light element microanalysis have been used to characterize both the deformation structures around indentations and the microchemistry of the films in terms of their oxygen and carbon contents. Attempts have also been made to correlate these observations with the nanoindentation data. In addition, the microhardness indentation response has been characterized to explore the extent to which the behaviour seen at contact loads in the range 0–60 mN extrapolates to higher load regimes.

While indentation experiments causing surface displacements of less than the coating thickness may yield data primarily concerning the coating, recent modelling work in our laboratory [10] suggests that the elastic or plastic reaction of the substrate together with membrane stresses in the coating (developed as the coating is stretched into the substrate) may become significant once surface deflections become greater than the coating thickness. Thus, in order to examine these effects, the range of indentation displacements should be up to at least twice the thickness of the coating.

Finally, nanoindentation experiments yield copious data from any single indentation cycle. Results from such data are best presented graphically (e.g. as load–displacement curves), as is the case here. However, the interpretation of such results immediately calls into question the meaning of parameters such as "hardness", especially for those cases in which the indenter does not cut through the coating but merely bends and stretches the coating into an impression primarily caused by plastic flow in the substrate [11]. Further, in those instances where the coating is bent into the substrate ahead of the indenter (see Section 3.2.2), the measured displacement of the indenter does not simply correspond to its being at that depth within the initial microstructure. Thus measuring properties as a function of depth becomes difficult. These problems are discussed further within the context of the observed behaviour and properties of the various films.

2. Experimental details

2.1. The samples

Two different a-C:H coatings were studied. Both were deposited on chemically polished (1 0 0) silicon wafers by an r.f.-PACVD process. The first was a nominally "hard" coating, ~ 230 nm thick, deposited from a methane–argon gas mixture, while the other was a ~ 210 nm thick, "soft" coating deposited from methane only. Deposition parameters are summarized in Table I.

TABLE I Deposition parameters and film thicknesses

Deposition parameters	"Hard" coating	"Soft" coating
Gas flow rates (sccm[a])	50 methane/100 argon	100 methane
Pressure (torr)	0.1	1
Power (W)	100	40
Deposition time (min)	35	7
Coating thickness (nm)	230	210

[a]Standard cubic centimetres.

For the "hard" coating, a strong Raman peak (using green laser light) was obtained at ~ 1500 cm^{-1}. However, because green light has a frequency very close to that of the sp^3 vibrational states, the signal was very enhanced. Hence although sp^3-bonded carbon is indicated to be present, the amount is uncertain. No Raman spectrum could be obtained for the "soft" coating because it luminesced and burnt away easily in the laser beam. For both coatings, infra-red reflectance spectroscopy showed the presence of CH_x: however, neither the amount nor the identity (CH_2, CH_3 or both) of this hydrocarbon could be deduced due to the very strong infra-red absorption by the silicon substrate.

2.2. Annealing

Specimens ~ 10 mm square were cleaved from the coated wafers and annealed in vacuum ($< 10^{-6}$ torr; 1 torr = 133.322 Pa) in the test chamber of a Wilberforce high-temperature microhardness testing machine for 30 min at various temperatures in the range 100–650 °C. Pre- and post-anneal examinations of the coating were carried out both by scanning electron microscopy (SEM) and by energy dispersive X-ray analysis (EDXA) using a Link System (LZ4/eXL) in conjunction with a CamScan S4-80DV scanning electron microscope.

2.3. Ultra-low-load indentation

Ultra-low-load indentation experiments were carried out using a Nano Indenter II mechanical properties microprobe (Nano Instruments Inc., Knoxville, TN, USA), at a thermally equilibrated temperature of 22 °C. Loads were varied over the range 0–60 mN, resulting in indentations up to ~ 600 nm deep in the softer carbon coating at peak load. The indenter was of a trigonal pyramid geometry (Berkovich indenter) with an end radius of curvature of ~ 100 nm. Experiments were carried out under load control conditions with a nominal loading and unloading rate of 50 $\mu\text{N s}^{-1}$. The machine was allowed to stabilize thermally so that the thermal drift of the test surface relative to the tip of the indenter was below 0.05 nm s^{-1} before the first indentation was made, this typically taking about 30 min. Any remaining drift could be compensated for with a "hold segment" in the indentation cycle (in this case at 70% unload), that is a period in which the partially loaded indenter remains at constant load, any changes in displacement being attributed to the residual thermal drift of the system enabling an average drift rate to be calculated (the possibility of any short-term indentation creep in these samples was ignored). All displacement data were then corrected using this drift rate, which was typically in the range 0.005–0.05 nm s^{-1}. Indentations were made in regular rectangular arrays, with 25 μm between impressions and between rows of impressions. These arrays enable easier recognition of indentations by SEM [9].

Load, displacement and time data from individual nanoindentation cycles were recorded digitally at regular intervals (approximately every 0.7 s) and were then processed to produce load–displacement graphs. From these, it is possible to calculate an indentation pressure (or "penetration resistance") as a function of depth. Although this might be thought of as the "hardness response", in the context of nanoindentation results the term is ambiguous and needs careful definition. This is because conventional "indentation hardness" is defined with reference to the size of the residual plastic impression measured after the test is complete and the load removed. This is clearly impossible to measure continuously during a nanoindentation load–unload cycle, although it is possible to obtain an instantaneous "hardness" value from the applied load and an area of contact calculated from the corresponding indenter displacement. However, this "load-on" hardness is not comparable with conventional hardness data (e.g. Vickers or Knoop microhardness) because it includes a contribution from the elastic flexure of the surface and therefore gives too large an indentation depth for a given load. In turn, this gives too large an area of contact, resulting in lower hardness values than would be obtained by conventional methods.

Doerner and Nix [12] have attempted to remove the elastic flexural contribution to the indenter displacement by calculating a plastic indentation depth for a given nanoindentation cycle. This is obtained by extrapolating the slope of the initial straight portion (about the first third) of the unloading curve to zero load. Because this does not allow for any depth recovery of the indentation itself, this resultant "plastic depth" is always greater than the final (residual) depth of the indentation as read from the load–displacement curve. This also tacitly assumes that the shape of the indenter–sample contact does not change during initial unloading (e.g. due to elastic recovery of the indenter itself), although this is experimentally difficult to confirm conclusively. While other approaches to the problem of calculating the contact area are in-hand [13], we have assumed that the approach of Doerner and Nix is acceptable in the present study and have used it for producing elastically corrected hardness (or "surface displacement resistance") values. However, a further complication is the possibility of a phase transformation during the indentation of silicon which might alter its elastic response particularly during unloading [9, 14].

Additionally, it is possible to obtain information regarding the elastic stiffness (as a function of indenter penetration) of the indenter–specimen contact from the Nasno Indenter II by superimposing a low amplitude a.c. signal at a frequency of about 150 Hz on the loading coil current, as described by Pethica and Oliver [15]. Although the capability is available to make these continuous contact stiffness measurements, the fact that the specimens are themselves coating–substrate composites, whose overall elastic moduli are quite likely to vary with depth, introduces extra complications that we are not yet able to deconvolute. Thus, we have taken a more qualitative approach to estimating the way in which the contact stiffness, as measured using the a.c. modulation method, varies between the different coatings. This has involved comparing the measured contact stiffness at the same indenter penetration (and therefore assuming approximately equal indenter geometry effects) and not calculating elastic moduli from these values. To try to obtain information primarily from the coating, two shallow depths, 50 and 100 nm, were chosen. Because the as-deposited coatings are of about the same thickness, this approach tacitly assumes that the (unknown) substrate contribution will also be approximately the same.

2.4. Microscopy and microanalysis

Following indentation experiments, all samples were examined by reflected light microscopy (RLM) which included imaging using Nomarski interference techniques. The initial large "range-finding" nanoindentations could usually been seen in this way and the rest of the array then indexed to it (even if beyond the resolution of the RLM methods) from the known spacings of the indentation array.

The same positions were sought using a software-driven stage of a CamScan S4-80DV SEM. Once located using high-probe current TV-rate images, higher resolution images were obtained at an accelerating voltage of 15 kV using probe sizes of ~ 10 nm with a probe current of ~ 40 pA from an LaB_6 source. The beam divergence was ~ 3 mrad. A liquid-nitrogen-cooled baffle was used to reduce the rate of contamination build-up on the sample (which was otherwise in a nominal vacuum of $\sim 1 \times 10^{-6}$ torr) so that long image-acquisition times could be used without noticeable image degradation. All samples were examined uncoated and at normal incidence (to reduce image distortion).

Microanalysis for oxygen and carbon was also undertaken using a Link LZ4 windowless EDXA detector and eXL spectral processing system on the CamScan SEM. For both the as-deposited and heat-treated samples, EDXA spectra were acquired at the same count rate (2800 counts s^{-1} at the CK_α peak) and to the same total peak count.

3. Results and discussion

3.1. Physical and compositional changes effected by annealing

After vacuum annealing at 400 °C, both coatings changed colour suggesting a change in the band structure (presumably due to hydrogen evolution [16]) but with no obvious change in surface appearance. However, while no detectable change (over the as-deposited state) was observed by SEM in the surface features of the "soft" coating over the entire temperature range, an interesting system of blisters or bubbles were observed in the harder coating after annealing at temperatures > 530 °C (see Fig. 1). Two types of blisters are apparent: the smaller are circular, whereas the larger blisters are "scalloped" around their edges. This suggests that there is a critical size

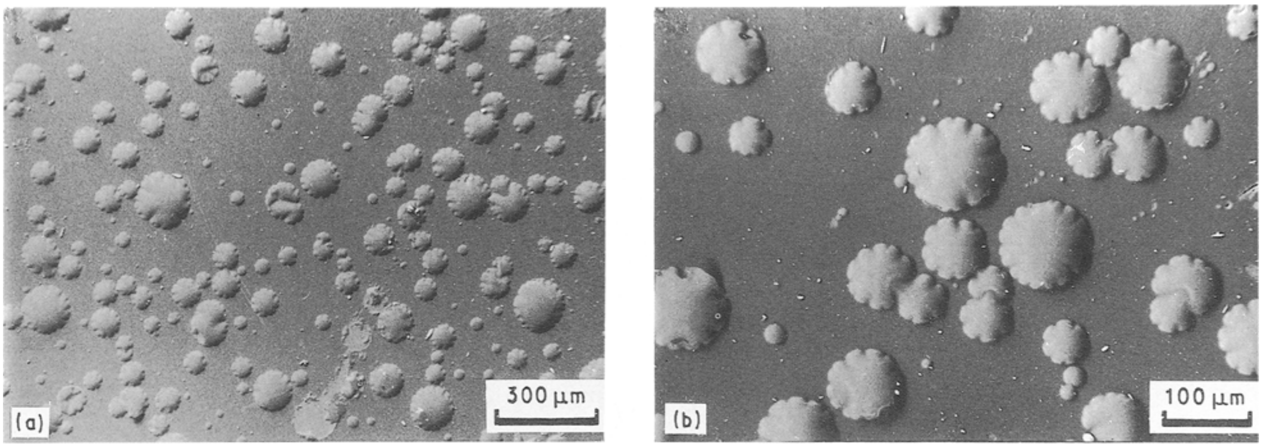

Figure 1 Scanning electron micrographs (secondary electron images, 20 kV) of dome-shaped blisters (believed to be argon bubbles) formed at the coating–substrate interface of the "hard" coated composite on annealing in vacuum at temperatures in excess of ~ 530 °C. While the larger blisters have scalloped edges, the smaller blisters are circular.

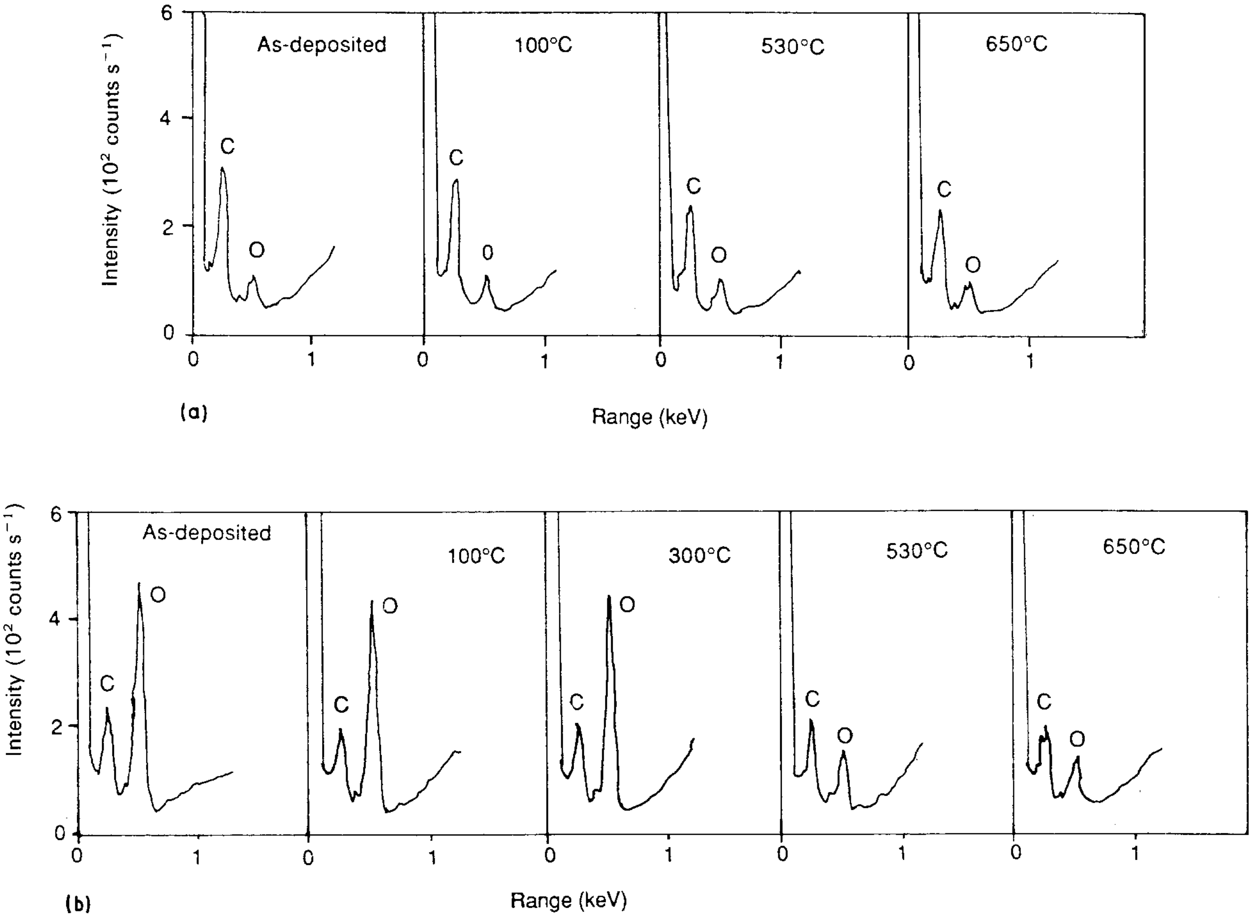

Figure 2 EDXA profiles of (a) the "hard", and (b) the "soft" coated composites in the as-deposited state and after annealing at the various temperatures indicated. Besides carbon, spectra from both coatings show the presence of oxygen, the oxygen peak being more pronounced relative to carbon for the "soft" coating. The relative oxygen:carbon ratios vary with heat-treatment (see text).

(and hence internal gas pressure) above which the change in appearance occurs, although the cause of this change has yet to be determined. As discussed in detail elsewhere [17], these bubbles are believed to contain argon originally trapped at the coating–substrate interface during deposition. However, of importance here is the fact that the easy formation of such bubbles in a hard, stiff, fairly brittle film is unlikely unless the film has developed soft, ductile (perhaps rubbery-polymer-like) properties at the higher heat-treatment temperatures (> 530 °C). Thus some resultant property changes (e.g. reduction of residual stress, changes in interfacial bond strength, etc.) might be expected on cool-down even though the film becomes hard and fairly brittle once again.

Fig. 2 shows typical EDXA spectra observed for both the "hard" and "soft" coating–substrate composites, respectively, in the as-deposited and heat-treated states. As can be seen in Fig. 2a, in addition to carbon, a small oxygen peak was observed for all the "hard" coated samples. Further, while the intensity of the oxygen peak remained essentially constant at the as-deposited value up to the 530 °C annealing temperature, that of the carbon was slightly diminished at and above this temperature.

Similar to the "hard" coating, oxygen was also detected in the "soft" coating (Fig. 2b). However, here the height of the oxygen peak is far larger, being about twice that of the carbon in the as-deposited sample and for the samples annealed at the lower temperatures. Also, there is a slight decrease (compared to the as-deposited state) of both the carbon and oxygen peaks after annealing at 100 °C. Thereafter the intensity of the carbon peak remains essentially constant up to the highest annealing temperature (650 °C), while at and above 530 °C the oxygen peak is drastically diminished compared to the lower annealing temperatures.

Because no oxygen was purposefully used during the deposition of either coating (see Table I) its presence in both coatings is presumed to result either from impurities in the precursor gases or from atmospheric adsorption (even though the amount, compared to carbon, present in the "soft" coating seems high). We have no evidence as to either the structural location or bonding of the oxygen within the films. However, as will be seen in Section 3.2, its liberation from the "soft" coating at the higher annealing temperatures is probably related to the drastic changes which occur in the nanoscale mechanical properties as a result of structural and interfacial bonding degradation.

TABLE II Displacement at various peak loads for the bare substrate and the as-deposited coatings

Peak load (mN)	Peak displacement (nm)		
	Substrate	"Hard" coating	"Soft" coating
1	37	35	100
2	58	51	155
5	110	100	210
10	175	160	290

3.2. Nanoindentation: loading and unloading characteristics

3.2.1. The as-deposited samples

Figs 3–5 show selected load–displacement curves for load–unload cyles for the bare silicon substrate (Fig. 3), and the "hard" (Fig. 4) and "soft" (Fig. 5) coated composites for maximum loads of 1, 2, 5 and 10 mN. Table II contains the displacement at maximum load for the bare substrate and the two as-deposited coatings as extracted from the graphs. From Table II and the graphs in Figs 3–5, the following observations can be made.

1. At the lowest maximum load (1 mN) the contact response of the "hard" coated composite is seen to be elastic (i.e. the loading and unloading curves appear coincident, as shown in Fig. 4a). By contrast the response of the bare substrate (Fig. 3a) and the "soft" coated composite (Fig. 5a) are elastic–plastic, i.e. the loading and unloading curves are not coincident and a residual displacement (corresponding to the depth of the plastic impression) is left in the sample following considerable elastic recovery during unloading.
2. For maximum loads greater than 1 mN, the "hard" coated composite exhibits increasing elastic–plastic behaviour.

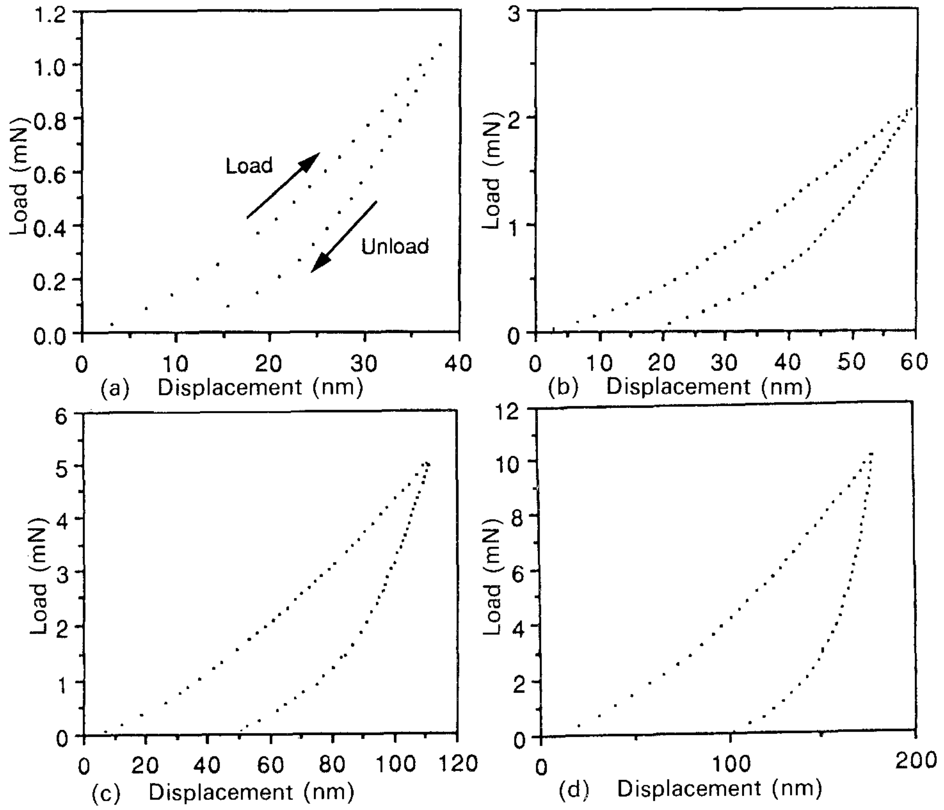

Figure 3 (a–d) The load–displacement nanoindentation response of the uncoated silicon substrate at maximum contact loads of 1, 2, 5 and 10 mN, respectively (see text).

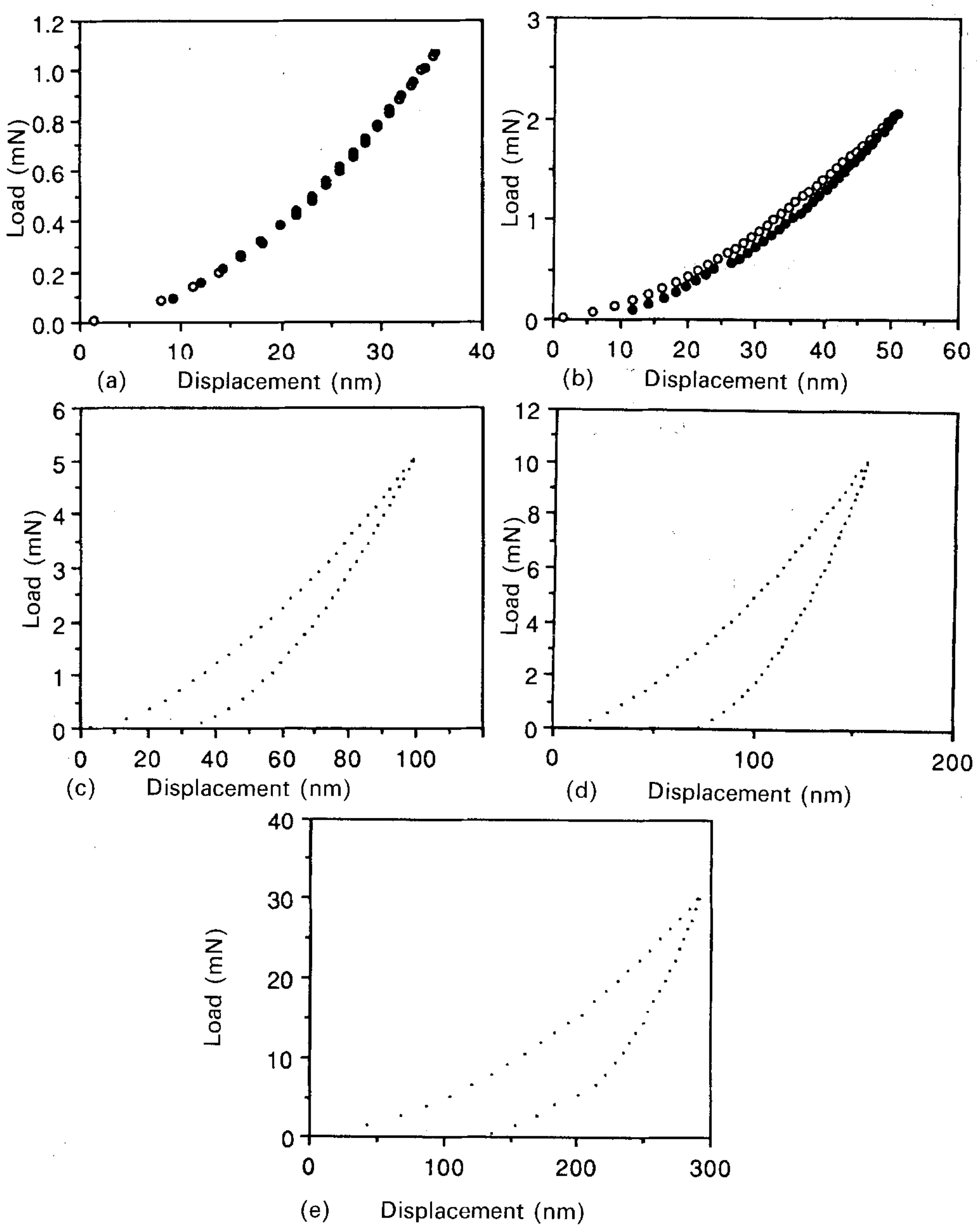

Figure 4 Load-displacement nanoindentation response for the "hard" coated composite. In (a) note that at a maximum load of 1 mN the response is almost completely elastic, i.e. the (○) loading and (●) unloading curves appear coincident. The loading and unloading curves become less coincident with increasing peak load (see text).

3. At corresponding loads, the penetration depth is always less for the "hard" coated composite and more for the "soft" coated composite than for the bare substrate. The same is also true for the area enclosed by the loading and unloading curves (which corresponds to the work of plastic deformation plus the energy stored at the elastic–plastic interface). The reverse trend holds for the elastically recovered depth, i.e. the "hard" coated composite recovers more than the bare substrate which in turn recovers more than the "soft" coated composite.

4. For penetration depths greater than the thickness of the coating (~ 230 and ~ 210 nm for the "hard" and "soft" coatings, respectively), the loading curves for the "soft" coated sample show a marked displacement discontinuity at a depth corresponding to the coating thickness (Fig. 5d). For the "hard" coated sample, however, no such marked discontinuity was observed.

From these observations it is clear that, compared to the bare substrate, the "hard" coating in the as-deposited state reduces the surface displacement by allowing less plastic deformation but a greater amount of elastic recovery. On the other hand, the "soft" coating, which exhibits far less elastic recovery and greater plastic deformation, is worse than the bare substrate.

The marked horizontal discontinuity observed in the loading curve of the "soft" coated composite at a penetration depth corresponding to the coating thickness (Fig. 5d) could be due to a number of effects. These include the coating being sufficiently ductile to be cut through by the indenter (which then sees a change in the mechanical response at the coating–substrate interface), the coating being softer or less dense closer to the interface, or an interlayer of softer material at the interface. A further possibility is the propagation of cracks both through the thickness of

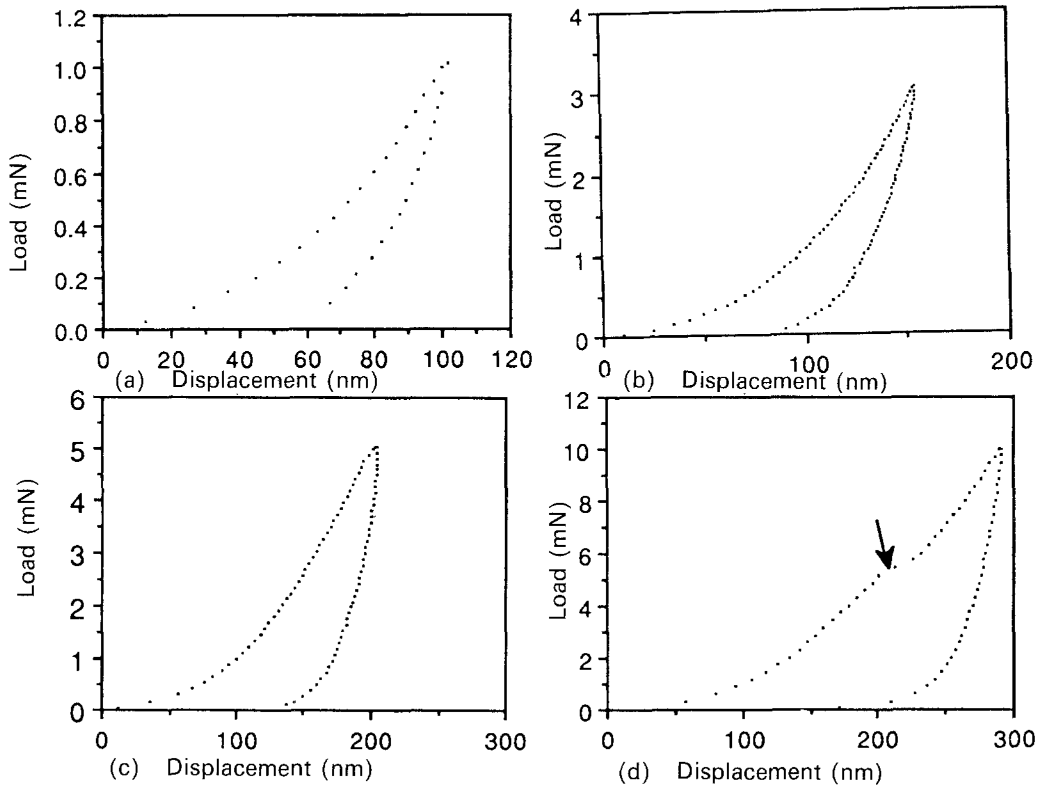

Figure 5 Load-displacement nanoindentation response for the "soft" coated composite. The loading and unloading curves are never coincident (i.e. significant plastic deformation occurs at all the applied loads used). Also, note the marked horizontal discontinuity (arrowed) in the loading curve of (d) where the indenter displacement corresponds to the thickness of the film (see text).

the coating and along the coating–substrate interface. As will be shown later such cracking is indeed observed and seems to be the most likely cause of the discontinuity. A simple increase in stiffness and penetration resistance as the indenter cuts through a soft coating on a harder substrate should appear as an increase in the slope of the load–displacement curve. This behaviour has been reported by Pollock *et al.* [7] for gold films on glass substrates. In the present work the discontinuity is different in that it appears as a discontinuous increase in the indenter displacement. This is probably due to the differing characteristics of the films: gold is soft but very ductile and therefore can be squeezed from beneath the indenter, whilst the "soft" a-C:H film is much less ductile and therefore cracks before it can be extruded out.

3.2.2. *Annealed samples*

Figs 6 and 7 show selected load–unload plots at various annealing temperatures (in the range 20–650 °C) for the "hard" and "soft" coated composites, respectively. The displacements at peak load are given in Table III. For the "hard" coated composite, the qualitative forms of the plots are essentially the same as those of the as-deposited sample at corresponding loads. However, for any given maximum load, a comparison of Fig. 6a–c and examination of Tables II and III show that, as the annealing temperature is increased, the maximum penetration depth and, to a lesser extent, the work of plastic deformation also increase, perhaps due to thermally induced microstructural degradation and/or residual stress relaxation (see later). On the other hand, the elastically recovered depth appears essentially unaffected by annealing.

Also of note are the slight horizontal discontinuities often observed in the loading curves of both the annealed (Fig 6b and c) as well as the as-deposited samples (Fig. 6a). The indenter displacements at which these occur are smaller than the coating thickness. The most likely interpretation of these events is that they represent the propagation of various types of cracks (either through the coating or along the coating–substrate interface) away from the immediate contact zone where the coating is flexed into conformity with the surface of the indenter, as shown schematically in Fig. 6d.

Two points are important here. The first is that the indenter displacements at which the discontinuities occur should not necessarily be interpreted as reflecting the position of the crack. Rather, the displacement is that required to create a critical stress (by stretching the coating, for example) for crack nucleation/propagation to occur somewhere. The most likely positions of through-thickness cracks caused in this way are in the regions of tensile stress either near the periphery of the indenter–surface contact zone or beneath the apex of the indenter as shown in Fig. 6d. The second point is that the occurrence of a through-thickness crack of the type shown immediately relaxes the membrane stresses developed in the film by stretching. These membrane stresses partly support the load on the indenter [10] and their relaxation causes the indenter to move to larger displacements, thus creating the displacement discontinuity observed.

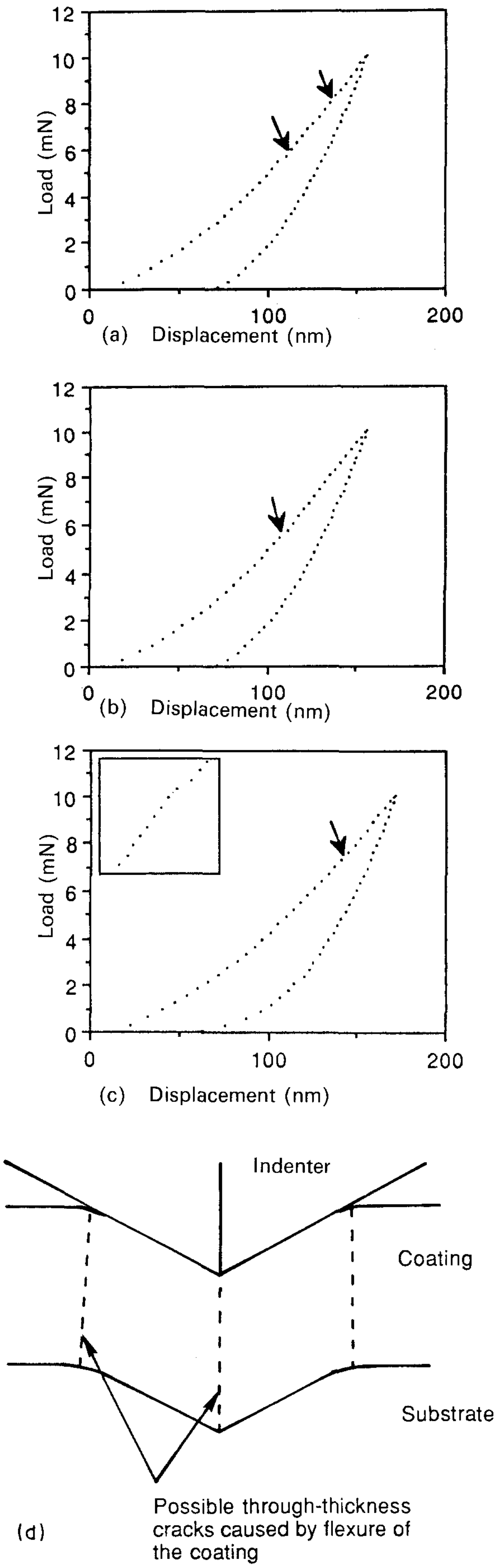

Figure 6 Typical load–displacement nanoindentation plots (at a maximum load of 10 mN) for (a) the "hard" coated composite in the as-deposited state, (b, c) after annealing at 100 and 530 °C, respectively. The slight discontinuities arrowed in the loading curves are due to cracking in the coating (see text). The inset in (c) shows such a discontinuity more clearly. (d) A schematic diagram of the location of cracks in the coating in response to the tensile "membrane stresses" caused by flexure of the coating around the indenter.

TABLE III Displacement at a peak load of 5 mN for the "hard" and "soft" coatings after heat treatment in vacuum at various temperatures

Heat treatment temperature (°C)	Peak displacement (nm)	
	"Hard" coating	"Soft" coating
As-deposited	100	210
100	100	227
300	[a]	225
530	110	225
650	130	175

[a] No specimen available.

In practice, these through-thickness cracks are also accompanied by interfacial debonding cracks (see Section 3.5.1).

For the "soft" coated composite (Table III and Fig. 7) the penetration depth, the elastically recovered depth and the work of plastic deformation show no systematic trend with increasing annealing temperature at corresponding loads: the peak displacement remaining the same for all but the sample annealed at the highest temperature. However, as the annealing temperature is increased, the marked discontinuity in the loading curve (initially observed at a penetration depth corresponding to the thickness of the coating in the as-deposited state) shifts to progressively lower penetration depths (from ~ 210 nm in the as-deposited state to ~ 190 nm at 100 and 300 °C, to ~ 125 nm at 530 °C and to ~ 110 nm at 650 °C). For the "soft" coating, microstructural observations of both nano- and microindentations suggests that interfacial debonding is very easy (see Section 3.5). Thus this particular discontinuity most probably corresponds to the propagation of an interfacial crack as the indenter cuts through the coating. To investigate this behaviour further, the depth at which the discontinuity occurred was plotted as a function of heat-treatment temperature and compared with the oxygen and carbon contents of the film also plotted as a function of heat-treatment temperature (Fig. 8). As can be seen from these plots, the behaviour of the discontinuity depth follows almost exactly the variation in oxygen content. Specifically, both show an initial decrease between 20 °C (the as-deposited sample) and 100 °C, followed by a plateau region between 100 and 300 °C, then a rapid decrease at the higher heat-treatment temperatures. By contrast the carbon content of the coating remains essentially constant over the heat-treatment temperature range.

The similarity between the oxygen content variation and the position of the discontinuity suggests that they are related. In particular, the conclusion must be that progressive liberation of oxygen from the coating with increasing heat-treatment temperature leads to progressive structural degradation (possibly including fine-scale porosity formation) as well as degradation of the interfacial adhesion (already very poor in the as-deposited state) which, in turn, leads to easier interfacial cracking and debonding at smaller levels of coating flexure. Hence the position of the discontinuity shifts to lower penetration depths as the annealing

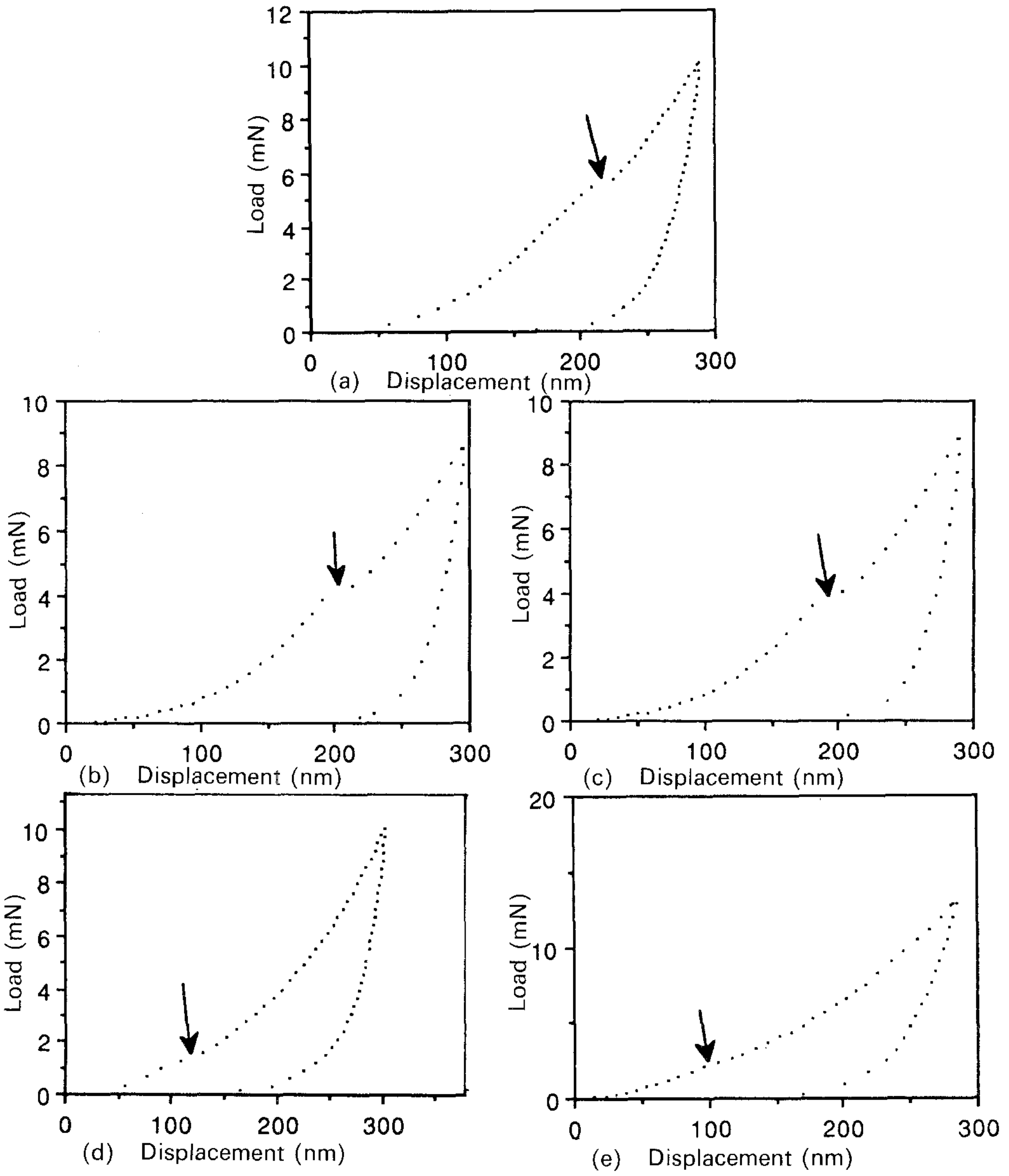

Figure 7 Load–displacement nanoindentation plots for the "soft" coated composite in (a) the as-deposited state and (b–e) after annealing at 100, 300, 530 and 650 °C, respectively. Note the shift to lower displacement (and lower load) of the discontinuity in the loading curves with increasing annealing temperature (see text).

temperature is increased. Thermally induced relaxation of residual stresses is ruled out as a contributory factor in the observed behaviour because, as reported elsewhere [17], this coating retained little or no compressive residual stress after deposition.

Finally, Fig. 9 shows that for relatively high indentation loads in the "soft" coating, the displacement depths at which the discontinuities in the loading curves occur are greater than the thickness of the coating (~ 230 nm). Because such displacement discontinuities are never observed in silicon at this load, the events observed here are most likely to be flexural-stress-induced cracks either through the coating or along the coating–substrate interface. This is a further example of the indenter displacement not necessarily reflecting the depth at which a particular deformation event is located.

3.3. Nanoindentation: surface displacement resistance

Fig. 10 shows "surface displacement resistance" curves for the bare substrate and for the "hard" and "soft" coated composites in the as-deposited state and after heat treatment at 530 °C. These curves are for the loading segment only and have been corrected for the elastic flexure of the specimen as described in Section 2.3 [12]. The important features of these curves are listed and discussed below.

1. For the bare substrate, the surface displacement resistance decreases with increasing penetration depth, the initial decrease (up to ~ 70 nm) being somewhat sharper than at larger penetrations where the curve shows a tendency towards levelling-off (Fig. 10a). Similar behaviour is also shown by the "hard" coated composite in both the as-deposited (Fig. 10b) and annealed (Fig. 10c) states, although the initial decrease below about 70 nm is less steep than is the case for the bare substrate. However, the response of the "soft" coated composite is far more complex, exhibiting both a maximum and two minima in the as-deposited as well as the annealed states (see Feature 4 below). The changes are presumed to be due to the increasing influence of the silicon substrate progressively supporting more of the load with increasing

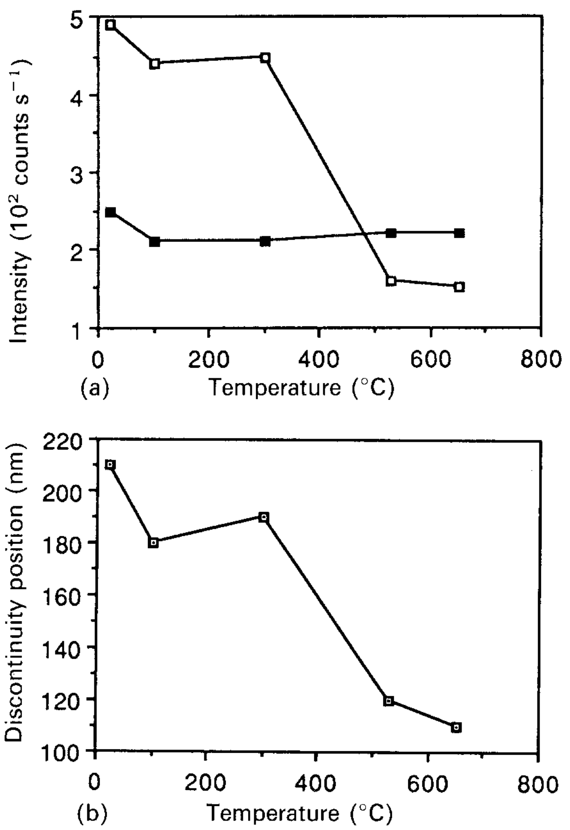

Figure 8 (a) Plots of the EDXA (□) oxygen and (■) carbon intensities (taken from Fig. 2) for the "soft" coated composite as a function of annealing temperature. (b) Plot of the position of the discontinuity in the loading curves of Fig. 7 as a function of the annealing temperature. Note that (b) follows the oxygen intensity plot of (a).

indenter displacement. Thus, in Fig. 10d, the penetration resistance increases towards the silicon value, even when the indenter displacement is less than half the thickness of the film (see [18] for a theoretical treatment of the influence of the substrate on the behaviour of the coating).

2. At corresponding penetration depths, the penetration resistance of the as-deposited "hard" coated composite is superior to that of the bare substrate which, in turn, exhibits higher values than the as-deposited "soft" coated composite.

3. For both coatings, heat-treatment at temperatures up to 530 °C causes a decrease in the surface displacement resistance compared with the as-deposited state (from ~ 32–50 GPa to ~ 26–40 GPa for the "hard" coating and ~ 4–6 GPa to ~ 4–5 GPa for the "soft" coating). Thermally induced microstructural changes (particularly due to the liberation of oxygen in the case of the "soft" coating) are expected to have a significant role in effecting the decrease, but for the "hard" coating a relaxation of all or part of the residual compressive stress (known to be present in the as-deposited coating [17]) probably plays a significant part.

4. For the "soft" coated composite, there is a second minimum in the hardness curves of Fig 10d and e. These are expected because of the displacement discontinuities discussed in Section 3.2.2 and are thus caused by the propagation of cracks.

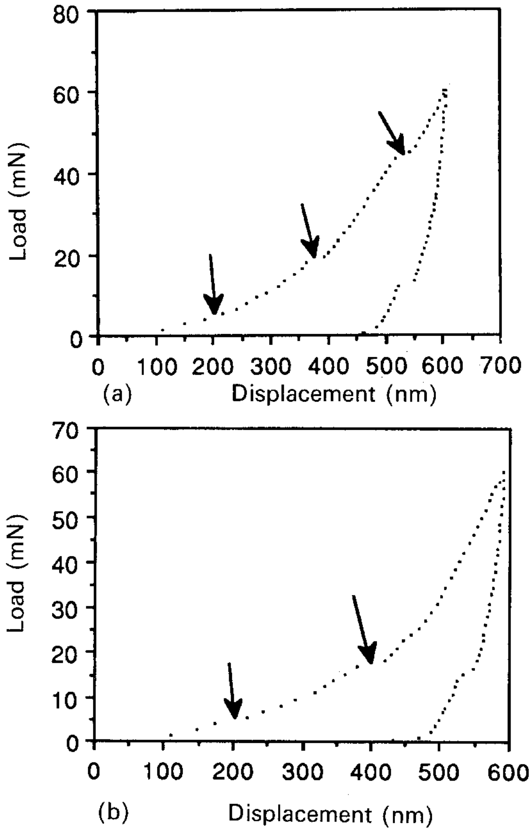

Figure 9 Load–displacement nanoindentation plots at a maximum load of 60 mN (which gives maximum displacements much greater than the thickness of the coating, ~ 210 nm) for the "soft" coated composite after annealing at (a) 100 °C and (b) 300 °C. The arrowed discontinuities indicate the occurrence of both through-thickness and interfacial cracks (see text). The steps in the unloading curve are related to a pressure-sensitive transformation occurring in the silicon [14].

TABLE IV Contact stiffness values determined using the superimposed a.c. modulation technique for the silicon substrate and the various "hard" and "soft" coated composites. Note that the values are for two indenter displacements, 50 and 100 nm, both chosen to be less than the thickness of the coatings

Sample	Heat treatment temperature (°C)	Contact stiffness (10^4 N m^{-1})	
		50 nm	100 nm
Si substrate	As-deposited	10	17.7
"Hard" coated composite	As-deposited	5.7	11.8
	100	5.8	11.1
	300	[a]	[a]
	530	5.0	9.9
	650	3.6	8.2
"Soft" coated composite	As-deposited	1.3	5.4
	100	1.4	4.7
	300	1.1	3.9
	530	–	5.0
	650	2.7	7.4

[a] No specimen available.

3.4. Nanoindentation: contact stiffness

The stiffness of the coating–substrate composite was monitored using the superimposed a.c. technique. For the reasons given earlier, these data have not been fully analysed. However, some selected values of contact stiffness at two fixed penetrations are given in Table IV.

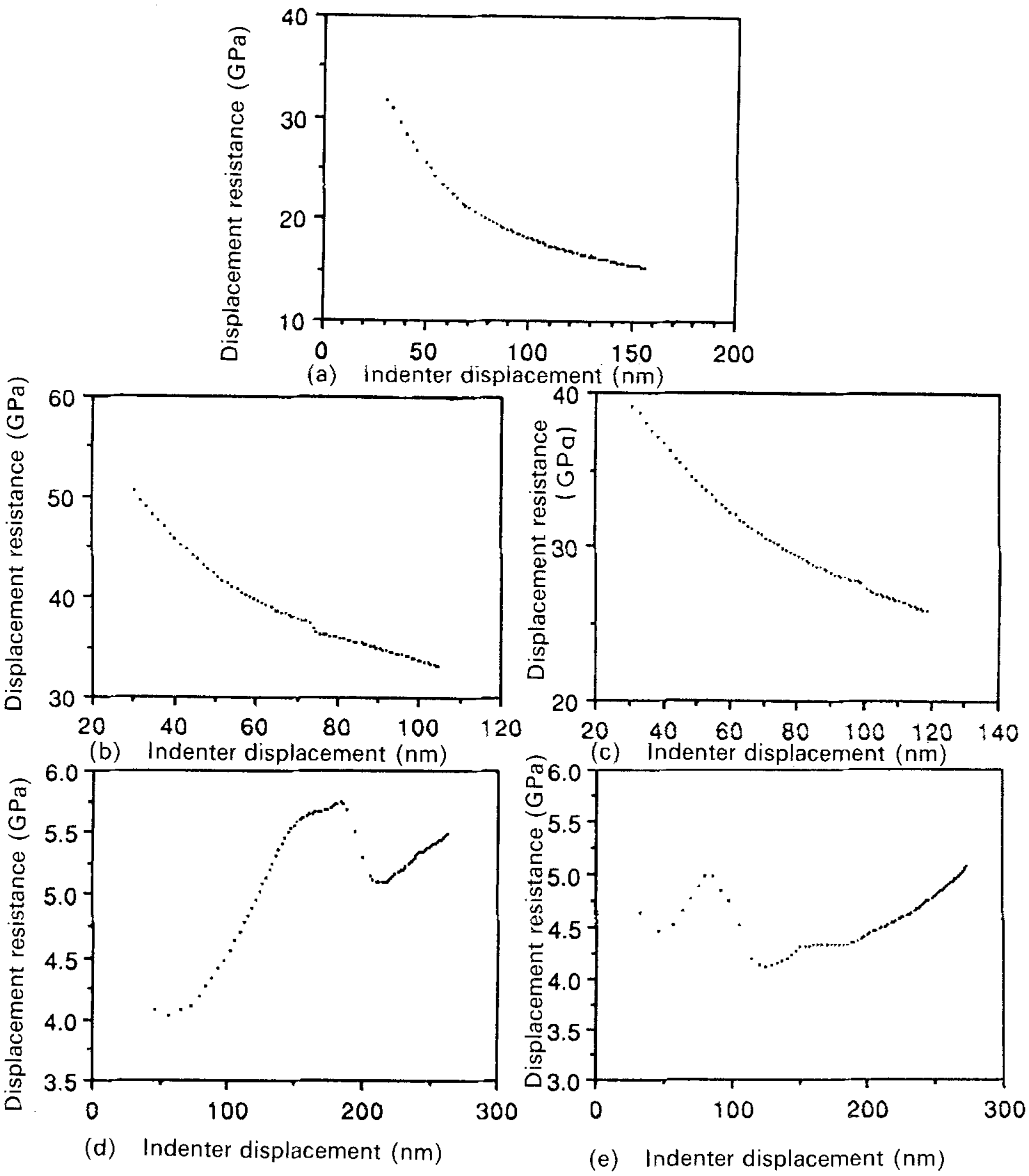

Figure 10 Surface "penetration resistance" versus depth plots for (a) the bare silicon substrate, (b, c) the "hard" coated composite in the as-deposited state and after annealing at 530 °C respectively, and (d, e) as (b, c) for the "soft" coated composite (see text).

Both of the as-deposited coatings had lower contact stiffness values than the uncoated silicon substrate, with the "soft" coated composite having the lowest contact stiffness at both indenter penetrations. Thus, while the "hard" coated composite is more penetration resistant than silicon, it appears to have a lower stiffness.

After heat-treatment at corresponding temperatures, the "hard" coated composite still yielded higher values than the "soft", although the two systems showed different trends. In the case of the "hard" coated composite, the contact stiffness dropped as the heat-treatment temperature was increased, perhaps suggesting a change in the structure of the film (e.g. the formation of microvoids reducing the integrity of the bond array). For the "soft" coated composite, the contact stiffness values initially fall from the as-deposited value and then rise to a value greater than the initial value after heat-treatment at the highest temperature. This behaviour could be due to reduction in the thickness of the film with increased heat-treatment temperature, resulting in a greater influence on the contact stiffness of the underlying substrate.

3.5. Microscopy

3.5.1. *Nanoindentations*

SEM imaging of nanoindentations is a challenging and time-consuming process, but is vitally necessary if the load–displacement data from a nanoindentation cycle are to be interpreted to reveal deformation mechanisms. For a:C-H, which is of low atomic number (and thus gives a poor secondary electron signal, large beam penetration and extensive beam broadening), it is only possible to observe satisfactorily the largest nanoindentations made here (i.e. those which are more than 2–3 μm across). Micrographs of these indentations are shown in Fig. 11. Smaller indentations can be imaged, but the detail tends to be lost because of the poor signal-to-noise ratio and beam spreading, even with an LaB_6 electron source.

In the case of the heat-treated "soft" coating, there is a circular disrupted zone surrounding the residual indentation. The disrupted zone almost extends as far from the centre of the indentation as the surface "crimps" which reveal where the edges of the trigonal indenter touched the surface when fully loaded. These "crimps" are caused by local plastic deformation in the

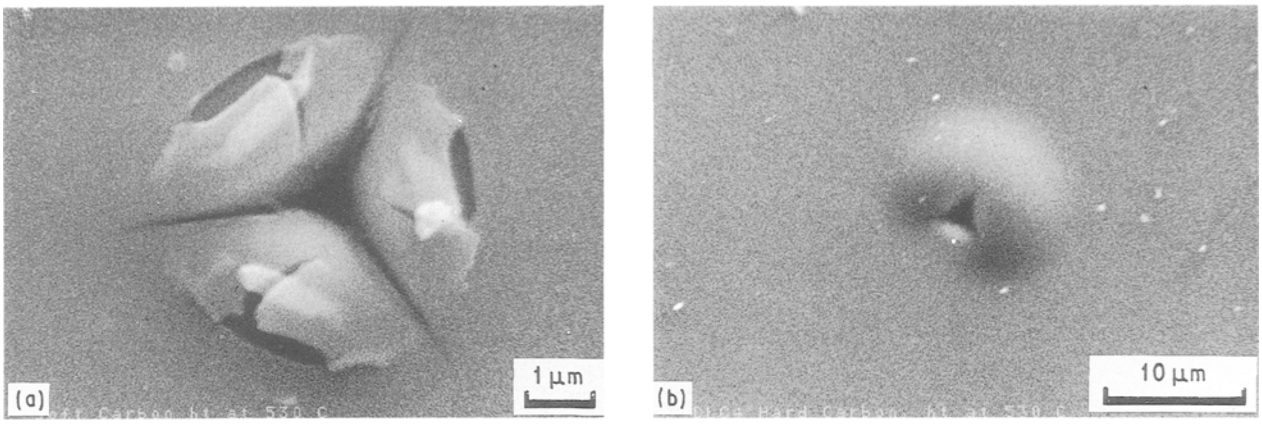

Figure 11 Scanning electron micrographs of high load (60 mN) nanoindentations in the (a) "soft" and (b) "hard" coated composites annealed at 530 °C. In (a) the extent of elastic recovery is discernible from the size of the central pyramidal impression relative to the extent of the "crimps" left in the surface by the edges of the indenter. In (b) the harder coating shows no such crimps, but always shows extensive interfacial debonding around the residual impression.

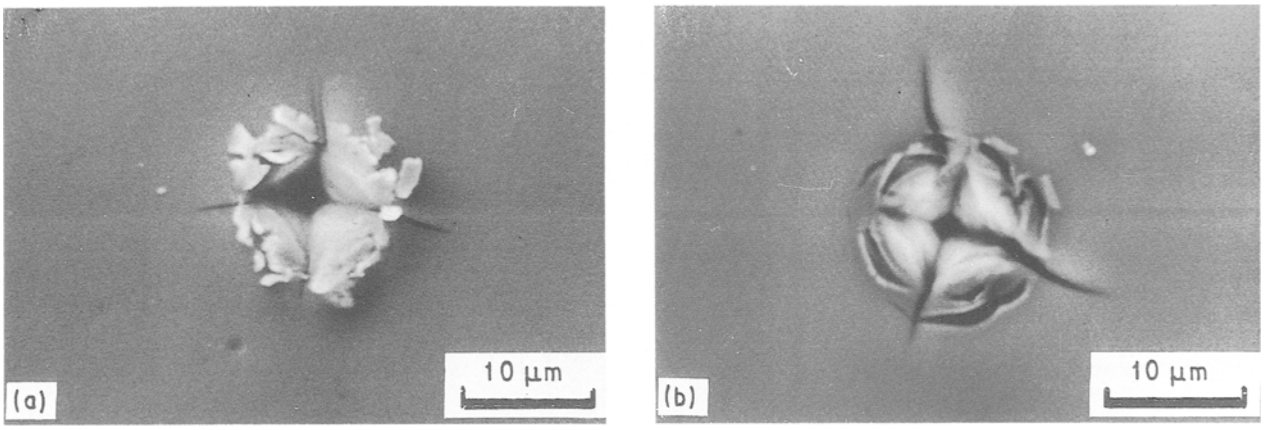

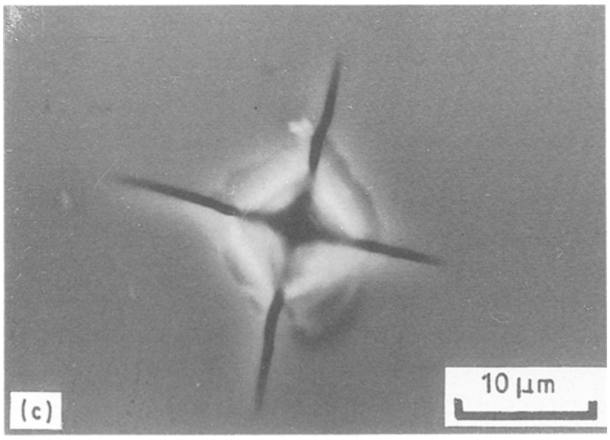

Figure 12 50 gF Vickers microhardness indentations made in the "soft" coated composite, (a) in the as-deposited state and (b, c) after annealing at 100 and 530 °C, respectively (see text).

very high stress regions associated with the edges of the indenter. Thus the fully loaded indentation diameter was ~ 5 µm (corresponding to an indentation depth of about 700 nm) while the residual central impression is only ~ 1 µm across. There appears to be extensive debonding within this zone, together with some spalling of the coating. The micrograph clearly indicates the very high level of elastic recovery which occurs in this system, the size of the residual indentation being very much smaller than the size of the loaded impression. This behaviour is typical of high-load nanoindentations in this system.

For the "hard" coating heat treated at 530 °C, the high-load (~ 60 mN) indentation has a very different appearance. Although the appearance of this smaller indentation is limited by image resolution, it is clearly surrounded by surface "bulge", presumably associated with the propagation of an interfacial crack allowing the coating to buckle upwards in response to the high levels of compressive stress remaining in the coating after annealing [17]. There is no visible cracking through the thickness of the coating and no spalling. The size of the blister in Fig. 11b is about 10 µm, with the residual indentation having a size of about 2.5 µm. Unlike the case of the soft coating, the edges of the indenter have not left a residual impression ("crimps") on the surface confirming the difficulty of plastic flow in this material. This behaviour appears to be characteristic because similar bulges were also observed around indentations produced using lower peak loads.

3.5.2. Microhardness indentations

In order to investigate whether the deformation mode of the coating changes with load, low-load (50 gF) Vickers microhardness tests were used (Shimadzu Model M Microhardness Tester) to monitor qualitative changes in the mechanical response of the coatings both in the as-deposited state and after annealing at

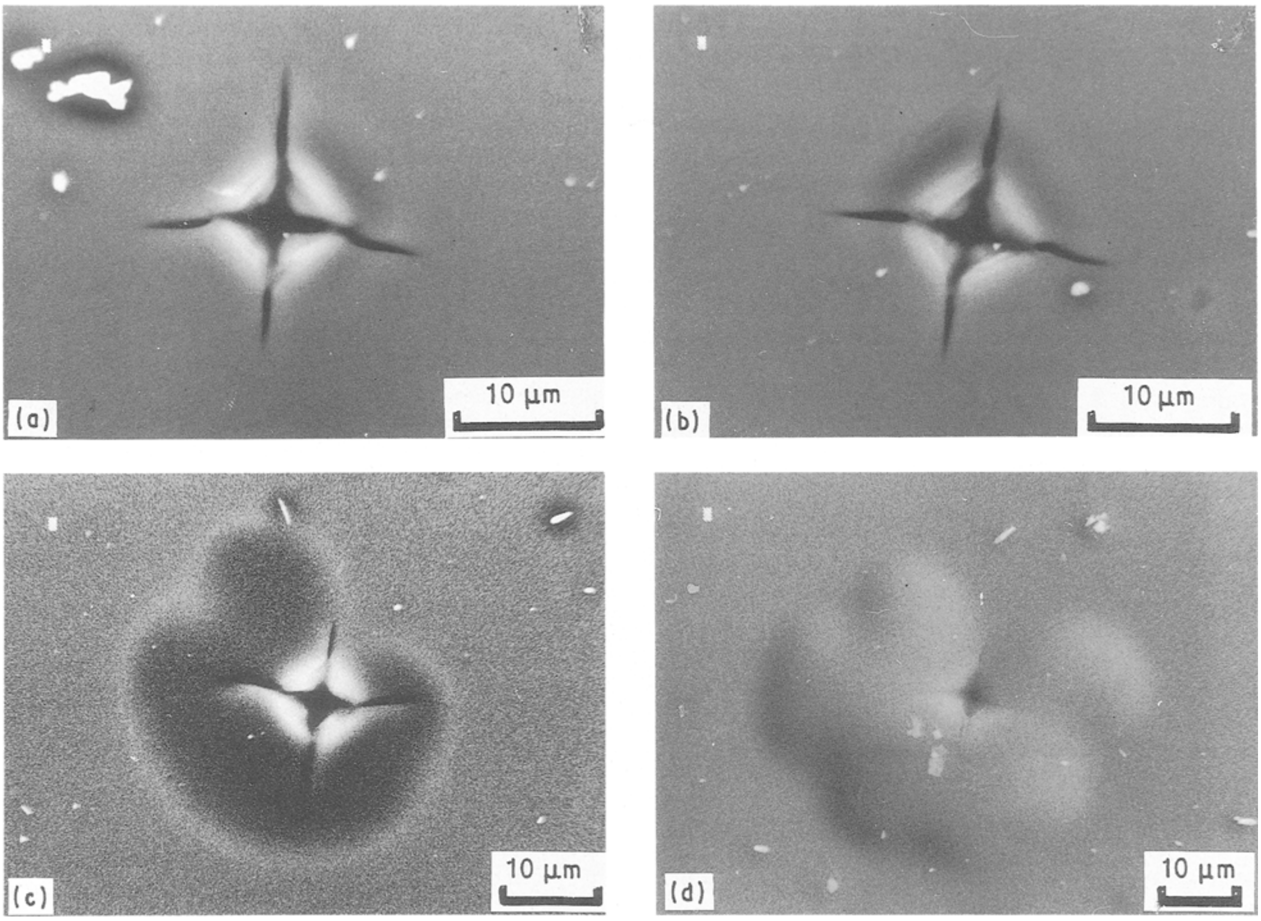

Figure 13 Scanning electron micrographs of 50 gF Vickers microhardness indentations made in the "hard" coated composite; (a, b) backscattered images in the as-deposited state and after heat-treatment at 100 °C, respectively; (c, d) are a backscattered electron image and a secondary electron image pair after annealing at 530 °C. As the heat-treatment temperature is increased, indentation-induced debonding of the coating, indicated by the dark areas around the indentations in (a–c) (and the bulged area in d), becomes more extensive (see text).

the various temperatures. Generally the results support the conclusions drawn from the nanoindentation experiments. For instance, it was observed that while indentation-induced cracking and debonding of the "soft" coating in the as-deposited state was limited (Fig. 12a), at annealing temperatures of 100 and 300 °C the cracking and debonding was more extensive (e.g. Fig. 12b), but without total removal of the coating (by spalling and fracture) outside the indentation. However, at the higher annealing temperatures (e.g. Fig. 12c) the coating spalled off completely, leaving the bare substrate exposed up to some 5 µm from the periphery of the residual indentation (cf. the nanoindentations where the spalling is only partial). These observations show that as the annealing temperature is increased both the interfacial bonding and the resistance of the coating to cracking are degraded.

Just as clearly as in Fig. 12, Fig. 13 shows the interfacial bonding between the "hard" coating and the substrate is also degraded with increasing annealing temperature. This was not explicitly evident from the nanoindentation probing, perhaps due to the interface being still sufficiently strong and tough at even the highest annealing temperature to withstand the small forces without failing.

4. Conclusions

1. Nanoindentation experiments clearly reveal the differing elastic and plastic properties of the two coatings when compared with each other and with the bare substrate. These highly localized *in situ* measurements also show how the properties of the coatings are changed by heat treatment.

2. Compared with the bare substrate, the "hard" coating in the as-deposited state enhances surface hardness, reduces surface displacement and exhibits less plastic deformation and greater elastic recovery. Through-thickness cracking of the coating is rare but interfacial debonding and buckling of the coating (presumed to be driven by residual stresses within the coating) often occur to form blisters around contact sites.

3. By contrast, the response of the "soft" coated composite appears to be worse than the bare substrate in all these areas. Further, even at loads as low as ~ 5 mN, the "soft" coated composite is susceptible to indentation-induced fracture and debonding along the coating–substrate interface.

4. From Conclusion 2 above, it is expected that if the nanoindentation response reflects the behaviour of contacting asperities during mild wear, then the presence of the "hard" coating will lead to better wear performance than the bare substrate.

5. Annealing in vacuum, even at moderate temperatures above room temperature, is detrimental to the structural integrity and interfacial adhesion of both

of the coatings. In the case of the "soft" coating the liberation of oxygen at the higher annealing temperatures appears to play the dominant role in structural and interfacial degradation, whilst for the "hard" coating, thermally induced relaxation of the residual stress (known to be present in the as-deposited coating) is also expected to play some part.

6. Commensurate with point 5, nanoindentation experiments clearly reveal the progressive worsening of the mechanical properties (e.g. hardness, elastic recovery, penetration depth, plastic deformation, etc.) of both coatings with increasing annealing temperature.

7. The contact stiffness measurements suggest that even the "hard", penetration-resistant, coating is less stiff than the silicon substrate. Further, the stiffness of the "hard" coated composite is reduced by heat treatment at progressively higher temperatures, whereas that of the "soft" coated composite decreases and then rises, suggesting increasing influence of the substrate.

8. Microstructural characterization of nanoindentations has been found to be a valuable means of interpreting load–displacement data, especially in confirming the extent of elastic recovery and the incidence of various types of crack.

9. Cracking of the coating during indentation leads to a discontinuity in the load–displacement curves, seen as an increase in indenter displacement for a given load.

Acknowledgements

J.C.K. acknowledges the support of the ICI plc Strategic Research Fund. The Materials Commission of SERC is acknowledged for the provision of the Nano Indenter II and for financial support (A.J.W.).

References

1. P. J. BURNETT and T. F. PAGE, *J. Mater. Sci.* **19** (1984) 845.
2. P. J. BURNETT and D. S. RICKERBY, *Surface Engng* **3** (1987) 69.
3. J. C. KNIGHT, T. F. PAGE and I. M. HUTCHINGS, *ibid.* **5** (1989) 213.
4. S. J. BULL and T. F. PAGE, *J. Mater. Sci.* **26** (1991) 3086.
5. J. B. PETHICA, in "Ion Implantation into Metals", edited by V. Ashworth, R. Proctor and W. Grant (Pergamon Press, Oxford, 1982) p. 147.
6. J. B. PETHICA, R. HUTCHINGS and W. C. OLIVER, *Phil. Mag. A* **48** (1983) 593.
7. H. M. POLLOCK, D. MAUGIS and M. BARQUINS, in "Microindentation Techniques in Materials Science and Engineering", edited by P. J. Blau and B. R. Lawn (American Society for Testing and Materials, Philadelphia, PA, 1985) p. 47.
8. M. F. DOERNER, D. S. GARDNER and W. D. NIX, *J. Mater. Res.* **1** (1986) 845.
9. T. F. PAGE, W. C. OLIVER and C. J. McHARGUE, *J. Mater. Res.*, **7** (1992) 450.
10. P. M. RAMSEY, H. W. CHANDLER and T. F. PAGE, *Surface Coatings Technol.* **49** (1991) 504.
11. T. F. PAGE and J. C. KNIGHT, *Surface Coatings Technol.* **39/40** (1989) 339.
12. M. F. DOERNER and W. D. NIX, *J. Mater. Res.* **1** (1986) 601.
13. W. C. OLIVER and G. M. PHARR, *J. Mater. Res.*, submitted.
14. A. J. WHITEHEAD and T. F. PAGE, *J. Mater. Sci.*, to be submitted.
15. J. B. PETHICA and W. C. OLIVER, *Mater. Res. Soc. Symp. Proc.* **130** (1989) 13.
16. P. M. FABIS, presented at the "18th International Conference on Metallurgical Coating and Thin Films", San Diego (1991).
17. J. C. KNIGHT, T. F. PAGE and H. W. CHANDLER, *Surface Coatings Technol.* **49** (1991) 519.
18. D. LEBOUVIER, P. GILORMINI and E. FELDER, *J. Phys. D* **18** (1985) 199.

Received 2 September
and accepted 10 September 1991